STRUCTURAL AND OPTICAL STUDIES OF WIDE BAND-GAP $Al_xGa_{1-x}N$ ($0 \leq x \leq 1$) SEMICONDUCTORS

NG SHA SHIONG

UNIVERSITI SAINS MALAYSIA

2007

STRUCTURAL AND OPTICAL STUDIES OF WIDE BAND-GAP $Al_xGa_{1-x}N$ ($0 \leq x \leq 1$) SEMICONDUCTORS

by

NG SHA SHIONG

Thesis submitted in fulfilment of the
requirements for the degree
of Doctor of Philosophy

October 2007

ACKNOWLEDGEMENTS

First of all, I would like to express my acknowledgment to my supervisor, Associate Prof. Dr. Zainuriah Hassan, for her guidance and supervision as well as patience throughout the course of my research. I would like to thank my co-supervisor, Associate Prof. Dr. Haslan Abu Hassan, for his interest and many invaluable suggestions and helpful comments during the preparation of this dissertation.

Secondly, I would like to thank all the assistance in NOR laboratory, especially: Mr. Kong Poh Quai, Ms. Ee Bee Choo, En. Mohtar Sabdin, En. Jamil Yusuf, and En. Muthalib Seikh Usman for their help and technical support offered during my laboratory work. I would also like to thank all of my friends, especially Dr. Yam Fong Kwong and Sin Yew Keong, for offering me assistance and sharing of information as well as discussion throughout this project.

I would also like to acknowledge IRPA RMK-8 Strategic Research Grant for supporting this work.

Finally, I would like to express my gratitude to my parents, for their full support and encouragement. A special thanks to my lovely wife, Ler Lee Hui, for supporting me from the beginning until the end.

TABLE OF CONTENTS

LIST OF TABLES

LIST OF FIGURES

LIST OF SYMBOLS

2θ-w	2theta-omega scan mode for XRD measurement
$\times$	Magnification
$\perp$	Direction perpendicular to C-axis
$\|\|$	Direction parallel to C-axis
β	Hexagonal wurtzite structure
α	Cubic zinc-blende structure
$\alpha_{a\,(c)}$	Thermal expansion coefficient perpendicular (parallel) to C-axis
γ	Phonon damping
$\varepsilon_{xx\,(yy)}$	Dielectric tensors perpendicular to C-axis
ε_{zz}	Dielectric tensors parallel to C-axis
ε_{∞}	High frequency dielectric constant
ε_0	Vacuum permittivity
$\varepsilon_{\parallel(\perp)}$	Dielectric function parallel (perpendicular)
$\varepsilon_{\infty,\parallel(\perp)}$	High-frequency dielectric constant parallel (perpendicular)
$\varepsilon_{0,\parallel(\perp)}$	Dielectric constant static parallel (perpendicular)
$\varepsilon(\mathrm{AC})_{\parallel,\perp}$	Dielectric constants parallel and perpendicular for AC binary compound.
$\varepsilon(\mathrm{BC})_{\parallel,\perp}$	Dielectric constants parallel and perpendicular for BC binary compound.
$\boldsymbol{k}_{\parallel}$	Wave vector of the of the incident radiation (or evanescent wave)
$\boldsymbol{k}_{\mathrm{vac}}$	Wave vector of the vacuum light wave
λ	Wavelength
λ_c	Critical wavelength
λ_{in}	Wavelength of the absorption photon
λ_{Abs}	Absorption edge
θ	Incident/diffraction angle
θ	Internal angle of incidence
θ_c	Critical angle
v	Poisson ratio
v_{AlN} (v_{GaN})	Poisson ratio of AlN (GaN)
v_i	Initial state
ν_{in}	Frequency of the incident photons
v_f	Final state
w	Angular frequency of the SP
w	Omega scan mode for XRD measurement
w_0	Frequency of the peak
w_s	Frequency of the surface excitation
w_{TO}	TO phonon frequency
w_{LO}	LO phonon frequency
w_{Al}	Weight percent of the Al element
$w_{\mathrm{E_1(TO)}}$	$\mathrm{E_1(TO)}$ phonon frequency
$w_{\mathrm{E_1(LO)}}$	$\mathrm{E_1(LO)}$ phonon frequency
$w_{\mathrm{A_1(TO)}}$	$\mathrm{A_1(TO)}$ phonon frequency

$w_{\mathrm{A_1(LO)}}$	$\mathrm{A_1(LO)}$ phonon frequency
w_{Ga}	Weight percent of the Ga element
w_p	Plasma frequency
Γ_0	BZ centre
Γ_{HM}	Full width at half maximum
ΔE	Difference in energy between two electronic states
$\Delta\mathrm{SPP}$	Average discrepancy between the experimental and theoretical SPP values
a	Lattice constant
a_0^{AlN} (c_0^{AlN})	Lattice constants a (c) of AlN
a_0^{GaN} (c_0^{GaN})	Lattice constants a (c) of GaN
$\mathrm{A_{1g}}$	Raman active mode of sapphire
$\mathrm{A_1(LO)}$	Phonon mode
$\mathrm{A_1(TO)}$	Phonon mode
A_{Al}	Atomic weight of the Al
A_{Ga}	Atomic weight of the Ga
b	Band gap energy bowing parameter
B	Phonon mode
c	Lattice constant
c	Velocity/speed of light
C	Crystallographic axis
C_{13} (C_{33})	Elastic modulus
d_{hkl}	Interplanar spacing between two consecutive scattering planes
e	Electron
e	Electron charge
$\boldsymbol{E}$	Electric field vector
$\mathrm{E_{1g}}$	Raman active mode of sapphire
$\mathrm{E_1(LO)}$	Phonon mode
$\mathrm{E_1(TO)}$	Phonon mode
$\mathrm{E_2(L)}$	Phonon mode
$\mathrm{E_2(H)}$	Phonon mode
E_a	Acceptor state
E_d	Donor state
E_g	Band gap energy
E_i	Intermediate state
h	Planck's constant
hkl	Miller indices
I	Intensity
I_0	Intensity at peak w_0
I_s	Integrated intensity of the peak
j	j-th oscillator
$\mathrm{K}_{\alpha 1}$	X-ray emission line
$\mathrm{K}_{\alpha 2}$	X-ray emission line
m	m-th order
m*	Effective mass of the electron
$\mathrm{m_e}$	Electron mass
n	Order of reflection
n	Refractive index
n_p	Refractive index of the Ge prism
N	Carrier concentration
$\boldsymbol{q}$	Wave-vector

r	Angle of refraction
R	Reflectivity
S	Phonon oscillator strength
t	Film thickness
T	Temperature
x	Al mole fraction / Alloy composition
x_{Al}	Al composition
x_{Ga}	Ga composition

LIST OF ABBREVIATIONS

2-D	2-dimensional
3-D	3-dimensional
arb. units	Arbitrary units
AFM	Atomic force microscopy
ATR	Attenuated total reflection
BL	Blue luminescence
BM	Brewster modes
BP	Bulk polariton
BSE	Backscattered electron
BZ	Brillouin zone
CB	Conduction band
CCD	Charge-coupled-device
CRT	Cathode ray display tube
DOS	Density of states
eV	Electron volt
e-beam	Electron beam
ECR	Electron cyclotron resonance
EDX	Energy dispersive x-ray
EW	Evanescent wave
FTIR	Fourier transform infrared
FWHM	Full width at half maximum
HR	High resolution
IR	Infrared
IRE	IR ellipsometry
IRE	Internal reflecting element
LDs	Laser diodes
LEDs	Light emitting diodes
LO	Longitudinal-optic
LP-MOCVD	Low pressure metalorganic chemical vapour deposition
LPP	LO plasmon-phonon
LST	Lyddane-Sachs-Teller
MBE	Molecular beam epitaxy
MM	Mixed mode behaviour
MOCVD	Metalorganic chemical vapour deposition
NA	Not available
NBE	Near band edge
NIRL	Near infrared luminescence
OM	One-mode behaviour
PA-MOCVD	Plasma-assisted metalorganic chemical vapour deposition
PL	Photoluminescence
RA	Reflection – absorption
RC	Rocking curve
RL	Red luminescence
RMS	Root-mean-squared
SE	Secondary electron
SEM	Scanning electron microscopy
SIS	Surface imaging systems
SP	Surface polaritons
SPP	Surface phonon polariton
TM	Two-mode behaviour

TO	Transverse-optic
UD	Unable to detect
UV	Ultraviolet
UV-VIS	Ultraviolet-visible spectroscopy
VB	Valence band
VIS	Visible
XRD	X-ray diffraction
YL	Yellow/orange-yellow luminescence

KAJIAN CIRI STRUKTUR DAN OPTIK BAGI SEMIKONDUKTOR BERJURANG TENAGA LEBAR $Al_xGa_{1-x}N$ ($0 \leq x \leq 1$)

ABSTRAK

Tujuan projek ini ialah untuk mengkaji ciri struktur dan optik bagi semikonduktor-semikondutor berjurang tenaga lebar $Al_xGa_{1-x}N$ ($0 \leq x \leq 1$) dengan pelbagai peralatan pencirian yang tak bersentuhan dan tak memusnahkan. Ini termasuklah mikroskopi imbasan elektron (SEM), serakan tenaga sinar-x (EDX), mikroskopi daya atomik (AFM) dan pembelauan sinar-x (XRD) untuk pencirian struktur, dan teknik pemantulan spectrum, spektroskopi ultraungu-cahaya nampak (UV-VIS), fotoluminesen (PL), spektroskopi Raman, spektroskopi pantulan inframerah (IR) terkutub dan pantulan penuh inframerah (IR) terkutub yang dilemahkan (ATR) untuk pencirian optik.

Kerja-kerja awal ke atas ciri struktur dan optik bagi filem-filem nipis GaN yang telah ditumbuhkan di atas pelbagai substrat, seperti substrat silikon (Si), batu nilam (Al_2O_3), gallium arsenida (GaAs), dan silikon karbida 6H (6H-SiC) telah dijalankan. Walau bagaimanapun, kajian-kajian ini telah difokuskan kepada pencirian PL dan Raman, kajian mendalam bagi asal-usul puncak berpantulan tinggi di dalam spektrum pantulan IR yang terkutub p, dan kajian XRD dan pantulan IR yang terkutub mengenai penghabluran bagi filem-filem nipis GaN yang ditumbuhkan atas substrat Si pada suhu substrat yang berlainan. Keputusan telah menunjukkan bahawa kualiti hablur yang lebih baik dapat diperolehi jika lapisan GaN ditumbuhkan atas substrat 6H-SiC. Tambahan pula, keputusan telah mendedahkan bahawa asal-usul puncak berpantulan tinggi di dalam spektrum pantulan IR yang terkutub p ialah mod fonon $TO_{\perp}$. Satu kolerasi di antara penghabluran dan bentuk jalur reststrahlen IR juga telah diperolehi.

Untuk semikonduktor-semikonduktor $Al_xGa_{1-x}N$, ketebalan dan komposisi aloi bagi filem-filem nipis $Al_xGa_{1-x}N$ telah ditentukan terlebih dahulu. Kajian-kajian terperinci ke atas kesan-kesan komposisi aloi, x, terhadap morfologi permukaan, kekasaran

permukaan, pemalar kekisi c dan kualiti hablur telah dijalankan. Tambahan pula, kesan-kesan pengaloian terhadap jurang tenaga asas E_g, mod-mod fonon optik pada pusat Brillouin zon (BZ) dan mod fonon polariton permukaan (SPP) telah disiasat dengan terperinci. Melalui kajian-kajian ini, keputusan-keputusan terhadap kelakuan dan kebersandaran terhadap komposisi bagi ciri-ciri asas struktur dan optik telah diperolehi atau diterbitkan. Bagi mod SPP, kelakuan satu-mod dan satu faktor lengkung ke atas (bagi persamaan kebersandaran terhadap komposisi) telah diperolehi. Adalah penting disebutkan bahawa ini merupakan kali pertama kelakuan dan kebersandaran terhadap komposisi bagi mod SPP aloi $Al_xGa_{1-x}N$ (begitu juga untuk aloi-aloi terner yang berstruktur wurtzit) diperolehi.

Secara keseluruhan, keputusan-keputusan telah mendedahkan bahawa pengaloian mempunyai satu impak yang besar ke atas ciri-ciri struktur dan optik bahan. Banyak ciri bagi aloi $Al_xGa_{1-x}N$ telah berubah dengan sepenuhnya dan berkelakuan dengan cara lain berbanding dengan bahan-bahan induk mereka, iaitu GaN (x = 0) dan AlN (x = 1). Akan tetapi, ciri-ciri bahan bagi aloi-aloi yang terbentuk adalah bergantung kepada komposisi aloi dan secara biasa dapat diwakilkan dengan satu interpolasi secara linear atau tak-linear antara unsur-unsurnya.

STRUCTURAL AND OPTICAL STUDIES OF WIDE BAND-GAP $Al_xGa_{1-x}N$ ($0 \leq x \leq 1$) SEMICONDUCTORS

ABSTRACT

The aim of this project is to study the structural and optical properties of wide band gap $Al_xGa_{1-x}N$ ($0 \leq x \leq 1$) semiconductors by means of various non-contact and non-destructive characterization tools. These include the scanning electron microscopy (SEM), energy dispersive x-ray (EDX) analysis, atomic force microscopy (AFM) and x-ray diffraction (XRD) for structural characterization, and spectral reflection technique, ultraviolet-visible (UV-VIS), photoluminescence (PL), Raman, polarized infrared (IR) reflectance and polarized IR attenuated total reflection (ATR) spectroscopy for optical characterization.

Initial works on the structural and optical properties of the GaN thin films grown on various substrates, such as silicon (Si), sapphire (Al_2O_3), gallium arsenide (GaAs), and 6H-silicon carbide (6H-SiC) substrates have been carried out. Studies are, however, focused on PL and Raman characterization and in-depth polarized IR reflectance study on the origin of the high reflection peak in the p-polarization spectrum as well as XRD and polarized IR reflectance studies on the crystallinity of GaN thin films. The results showed that a better crystalline quality can be achieved if the GaN layer is grown on 6H-SiC substrate. In addition, the results revealed that the origin of the high reflection peak in the p-polarization IR reflectance spectrum is the $TO_{\perp}$ phonon mode. A correlation between the crystallinity and the IR reststrahlen band shapes has also been obtained.

For $Al_xGa_{1-x}N$ semiconductors, the thickness and the alloy composition of the $Al_xGa_{1-x}N$ thin films are first determined. Thorough studies on the influence of the Al composition, x, on the surface morphology, surface roughness, lattice constant c and the crystalline quality are conducted. In addition, alloying effects on the fundamental band gap energy E_g, the Brillouin zone (BZ) centre optical phonon modes and the

surface phonon polariton (SPP) mode are investigated thoroughly. Through these studies, a number of results on the behaviour and composition dependence of the fundamental structural and optical characteristics have been obtained or derived. For the SPP mode, a one-mode (OM) behaviour and an upward bowing factor (for the composition dependence equation) have been obtained. It is important to note that this is the first time the behaviour and the composition dependence of the SPP mode of the $Al_xGa_{1-x}N$ alloy (as well as the wurtzite structure ternary alloys) are obtained.

Overall, the results revealed that the work of alloying has a great impact on the structural and optical characteristics of the materials. Many properties of the $Al_xGa_{1-x}N$ alloy have been completely changed and behave differently as compared to their parent materials, namely, the GaN (x = 0) and the AlN (x = 1). However, the material properties of the alloy materials formed are dependent on the alloy composition and typically can be represented by a linear or non-linear interpolation between its constituents.

CHAPTER 1

INTRODUCTION

1.1 Introduction

Owing to the outstanding optical properties such as wide range band-gap energy and high emitting performance, group-III nitride semiconductors such as aluminium nitride (AlN), gallium nitride (GaN), indium nitride (InN) and their alloys have attracted both academic and technological extensive research in recent years. As a consequence, efficient green-blue-ultraviolet light emitting diodes (LEDs), blue-violet laser diodes (LDs) and ultraviolet (UV) detectors as well as high voltage, high temperature and high frequency electronic devices have been successfully realized (Nakamura, 1999; Kung and Razegui, 2000; Asif Khan et al., 1994; Shur et al., 1999).

Group-III nitride ternary alloys, particularly aluminium gallium nitride (AlGaN) have been recognized to have the potential for applications in semiconductor light emitting devices and solar-blind UV detector as well as sensor devices, particularly for operating under harsh environment conditions (Shur et al., 1999; Gotthold and Guo, 2003; Razeghi, 2002; Allerman et al., 2003; Munoz et al., 2001; Mukai et al., 2001). Besides that, it also has the capacity to cover the spectrum from visible (VIS) to deep UV spectral range. These are strongly driven by their superior physical properties such as excellent thermal, mechanical and chemical stability, and unique optical properties such as direct and tuneable band gap energy (ranging from 3.4 to 6.2 eV).

Although great progress has been achieved in the fabrication of AlGaN-based devices, little is known about their fundamental materials properties. As compared to its family, the physical properties of III-V nitrides binary semiconductors have been reviewed in-depth and summarized in many books (Adachi, 2005; Ruterana, Alberecht

and Neugebauer, 2003; Levinshtein, Rumyantsev and Shur, 2001; Pankove and Moustakas, 1999; Morkoc, 1998; Pearton, 1997) as well as technical papers (Reshchikov and Morkoc, 2005; Jain et al., 2000; Pearton et al., 1999; Ambacher, 1998; Mohammad and Morkoc, 1996; Strite, Lin and Morkoc, 1993).

For AlGaN alloys, many attentions have been paid to the device applications. For the fundamental material properties, most of the works are devoted to the determination of the band gap energy bowing parameter b as well as the behaviour of the optical phonon modes as a function of Al composition. Despite these findings, there is no consensus between the literature results concerning these subjects. This is mainly due to the differences in the sample quality and the narrow range of the alloy compositions that are explored. Apart from that, many basic physical properties still remain unclear or unexplored. For instance, knowledge on the surface phonon polariton (SPP) modes, which is crucial for understanding the behaviour of the coupling effect between the photon and surface phonon, is still rare and has not received sufficient attention. Hence, from both the fundamental physics point-of-view and the potential application of the nitrides semiconductor, there is an absolute need for thorough studies on the fundamental properties of these materials.

In order to contribute to the understanding of the fundamental properties of this advanced material as well as the advancement of knowledge in the condensed matter, the influences of the Al composition on the structural and optical as well as surface properties of this ternary alloy will be investigated.

1.2 Research objectives

In this work, initial investigation is focused on the detailed studies of the structural and optical properties of the GaN thin films. The aims of these studies are to characterize the optical properties of the GaN thin films grown on various substrates

and to perform an in-depth study of the origin of the high reflection peak in the p-polarization infrared (IR) reflectance spectrum. The objective of these studies also includes the investigation of the correlation between the crystalline quality and the variations of IR reststrahlen band of a set of GaN thin films (with a variety of structural or crystalline quality) grown on silicon (Si) substrates at various substrate temperatures.

In general, these preliminary works eventually provides a better understanding on the fundamental properties for the subsequent study of the wide band gap $Al_xGa_{1-x}N$ ($0 \leq x \leq 1$) semiconductors, and hence facilitates the characterization research as well as the analyses of the obtained results.

Thorough studies on structural and optical characteristics of $Al_xGa_{1-x}N$ ($0 \leq x \leq 1$) semiconductors have been carried out by means of various non-contact and non-destructive characterization tools. These include the scanning electron microscopy (SEM), energy dispersive x-ray (EDX) analysis, atomic force microscopy (AFM), x-ray diffraction (XRD), spectral reflectance technique, ultraviolet-visible (UV-VIS) spectroscopy, photoluminescence (PL) spectroscopy, Raman spectroscopy and polarized IR reflectance spectroscopy as well as polarized IR attenuated total reflection (ATR) spectroscopy. The main research objectives are to investigate the effects of the alloys composition, x, on the surface morphology, the surface roughness, the lattice constant c, and the crystalline quality of the $Al_xGa_{1-x}N$ ($0 \leq x \leq 1$) thin films. Besides that, the research objectives also included investigations of the alloying effects on the fundamental band gap energy E_g, the behaviour of the Brillouin zone (BZ) centre optical phonon modes, particularly the $E_2(L)$, $E_1(TO)$, $E_2(H)$ and $A_1(LO)$, and the behaviour of the SPP mode of the $Al_xGa_{1-x}N$ ($0 \leq x \leq 1$) thin films. Determinations of the composition dependence equation of these characteristics in the entire Al composition range are carried out in parallel with the above characterization studies.

1.3 Originality of the research works

The main originality of this research work lies in the experimental and theoretical studies of the influences of the alloy composition, x, on the SPP mode of the $Al_xGa_{1-x}N$ ($0 \leq x \leq 1$) thin films. Through this research study, the composition dependence and the behaviour of the SPP mode of the $Al_xGa_{1-x}N$ ($0 \leq x \leq 1$) thin films are reported for the first time.

Apart from that, the alloying effects on the surface morphology and the surface roughness, the lattice constant c and the crystallite quality, the fundamental band gap energy E_g, and the behaviour of the BZ optical phonon modes of the $Al_xGa_{1-x}N$ thin films have been investigated thoroughly over the entire Al composition range ($0 \leq x \leq 1$). Through this sequential study, many previously reported experimental results have been confirmed or verified. Moreover, some new findings, mainly the composition dependence equation for the optical phonon modes, have been derived.

On the other hand, the results of this research project have also led to new explanations of the origin of the optical phonon modes that can be obtained through the oblique incident polarized IR measurements on the wurtzite nitrides. In addition, an alternative technique to determine the crystallinity of the deposited films based on the IR reflectance measurements has also been proposed.

1.4 Organization of dissertation

Generally, the content of this dissertation is organized as follows.

In Chapter 2, early studies on the structural and optical properties of the AlGaN semiconductor are reviewed. However, emphasis will be placed on the band gap energy bowing parameter b, the behaviour of the BZ optical phonon modes and the

SPP mode. Apart from that, an overview of the assignment of the IR optical phonon modes will be presented in this chapter.

Chapter 3 is devoted to the fundamental properties of the GaN and the AlN as well as the $Al_xGa_{1-x}N$ semiconductors. Theoretical models used to fit/generate the PL, the Raman, the polarized IR reflectance and the SPP spectra of the $Al_xGa_{1-x}N$ semiconductors are also included.

In Chapter 4, the general principles underlying the operation of the characterization tools and the experimental details for each characterization work are discussed. These include the samples details, experimental set-up and the operating conditions as well as the resolution.

In Chapter 5, the results and discussion for the PL and Raman characterization of the GaN thin films grown on various substrates, namely, sapphire (Al_2O_3), 6H-silicon carbide (6H-SiC), gallium arsenide (GaAs) and Si are presented. In-depth polarized IR reflectance analyses, with emphasis on the GaN thin film grown on 6H-SiC substrate, are also given.

Chapter 6 discusses the results of the XRD and polarized IR reflectance characterization of a set of GaN thin films grown on Si substrate at various substrate temperatures.

Chapter 7 contains the structural and optical studies of the $Al_xGa_{1-x}N$ ($0 \leq x \leq 1$) semiconductors. The results and discussion is mainly devoted to the influence of alloying on the structural and optical properties of the $Al_xGa_{1-x}N$ semiconductors.

Finally, in Chapter 8, conclusions on the characterization results covered in this dissertation and recommendations for future research are given.

CHAPTER 2

LITERATURE REVIEW

2.1 Introduction

In this chapter, the overview of the IR active optical phonon modes of wurtzite GaN thin films in the polarized spectra will be discussed briefly. Next, the present status of the characterization studies of the $Al_xGa_{1-x}N$ semiconductor will be reviewed. Emphasis will be placed on the band gap energy bowing parameter b, the behaviour of the BZ optical phonon modes, and the SPP mode of the $Al_xGa_{1-x}N$ semiconductor. In the final section of this chapter, a concluding remark of these literature reviews is presented.

2.2 Overview on IR active optical phonon modes of wurtzite GaN thin films in the polarized spectra

Up to now, a number of studies on the optical properties of the GaN in the IR region have been carried out by measuring the reflectivity of the thin films for radiation at normal or oblique incidence (Perlin et al., 1995; Perlin et al., 1996; MacMillan et al., 1996; Yu et al., 1998; Iller et al., 1999; Hou et al., 1999; Deguchi et al., 1999; Li et al., 1999; Frayssinet et al., 2000; Hou et al., 2000; Feng, Yang and Hou, 2001; Feng et al., 2002; Zhang et al., 2001). Since wurtzite structure GaN is a uniaxial crystal, two sets of phonon parameters are required to describe the dielectric function, namely, one set to model $\varepsilon_{\perp}$ and another set to model $\varepsilon_{\parallel}$ (Barker and Ilegems, 1973). As a result, these experimental data provided fairly little information as compared to polarized

measurements. According to Dumelow et al. (1993), the materials parameters can be determined more accurately if the reflectance measurements are performed by means of the oblique incidence polarized light. This is owing to purely transverse-optic (TO) and longitudinal-optic (LO) phonon modes can be observed for phonons propagating in the direction perpendicular ($\perp$) and parallel ($\|$) to the crystal axis, C, respectively; hence, more strongly marked features can be obtained. Consequently, more informative and accurate results can be obtained through the polarized measurements.

To date, detailed investigations of the polarized IR reflectance on GaN have been reported by Barker and Ilegems (1973), Manchon et al. (1970), Sobotta et al. (1992), Hao et al. (1999), Wetzel et al. (1996), Mirjalili et al. (1996, 1998) and Yu, Rowell and Lockwood (2004) research groups. Besides that, there are numerous polarized IR ellipsometry (IRE) measurements on GaN thin films, however, the interpretation of the spectra and the ways to extract the lattice vibrational parameters are different as compared to typical polarized IR reflectance analysis. Thus, it will not be discussed here.

The early investigation of the GaN thin films (most probably of poor quality) by Barker and Ilegems (1973) and Manchon et al. (1970) resulted in the determination of the optical parameters with large uncertainty. Sobotta et al. (1992) measured GaN samples with crystallographic C-axis along the plane of the layers. Consequently, they were able to determine the optical parameters from the reflectivity spectra exactly for the polarizations perpendicular ($\boldsymbol{E} \perp C$) and parallel ($\boldsymbol{E} \parallel C$) to the C-axis. (It is important to note here that, the results obtained both in this study and in all the IR studies quoted here are different from Sobotta et al. (1992) because the GaN samples with the C-axis oriented along the growth direction have been used.) Hao et al. (1999) had studied on the polarized transmission and reflection measurements of bulk GaN, but their analyses were mainly on the determinations of absorption coefficient and refractive index. Wetzel et al. (1996) studied the polarized IR reflection of heterostructures of GaN and AlGaN thin films with AlN buffer layers. However, their studies were mainly

focused on the LO phonon modes of the GaN and AlN. Polarized IR measurements of GaN films with various structures, which were deposited on various substrates, were reported by Mirjalili et al. (1996, 1998). However, as commented by Huo et al. (1999), the simulated spectra do not exactly fit the experiment well enough. For Yu, Rowell and Lockwood (2004), a study was done on the polarized IR reflection of GaN epilayer grown on sapphire substrate at three different angles of incidence (18°, 45° and 75°). Their studies were mainly focused on the fitting of numerical first differential reflectance by using a factorized model of dielectric constant and more attention was paid to the sapphire. For GaN thin films on sapphire, they were unable to observe and fix the $A_1(TO)$ phonon mode (as quoted by the authors); hence, an $A_1(TO)$ mode with a large uncertainty was obtained.

Commonly, all these polarized IR studies are able to determine a set of TO (⊥ and ||) and LO (⊥ and ||) phonon modes for both $\boldsymbol{E} \perp C$ and $\boldsymbol{E} \parallel C$. Principally, the $TO_{\perp}$ and the $LO_{\parallel}$ are first obtained from the best fits of the theoretical model to the experimental curve, then Lyddane-Sachs-Teller (LST) relation (Lyddane, Sachs and Teller, 1941) is applied to calculate the corresponding $LO_{\perp}$ and $TO_{\parallel}$. Up to now, good agreement has been obtained between these reported results and there are no doubts about the reported results. However, it seems that the fundamental principle of the IR phonon coupling has not been taken into consideration. It is well known for typical IR measurements that the wave-vector ($\boldsymbol{q}$) of the radiation may be taken as zero ($\boldsymbol{q}$ = 0). This is often referred to as the “long-wavelength limit” or “zone-centre” approximation (Houghton and Smith, 1966; Moller and Rothschild, 1971). Consequently, the optical phonon modes that can be detected are those coming from the BZ centre only, namely, the $TO_{\perp}$ and the $LO_{\parallel}$; while the BZ edge modes of $LO_{\perp}$ and $TO_{\parallel}$ are forbidden. Note that the condition $\boldsymbol{q} = 0$ holds also for Raman scattering (Moller and Rothschild, 1971). As a result, there is a need to look into the details of the interpretation of the polarized IR reflectance spectra and the use of the LST equation for determinations of the $LO_{\perp}$

and the $TO_{||}$ phonon modes. Furthermore, through the in-depth studies, it is found that the origin of the transverse-optic ($TO_{||}$) phonon mode in the p-polarized spectrum thus far is inappropriate. Based on Balkanski IR theory for thin films (Balkanski, 1972), Fresnel formulae for the oblique incidence polarized IR reflectivity, and vector analysis of the polarized IR incident beam, it can clearly confirm that this mode actually has the same origin as the TO mode in s-polarized spectrum and can be attributed to the $TO_{\perp}$ optical phonon mode. A detailed discussion will be given in Chapter 5.

2.3 Overview on the characterization studies of $Al_xGa_{1-x}N$ semiconductor

As mentioned in Chapter 1, much of the works on the AlGaN alloys are devoted to the device applications. For the fundamental material properties, although there are a number of studies, it is found that there is no consensus among the literature results concerning the band gap energy bowing parameter b and the behaviour of the BZ optical phonon modes. For SPP mode of the $Al_xGa_{1-x}N$ semiconductor, the research in this field is still rare and has not received sufficient attention. This is even true for the case in GaN (x = 0) and AlN (x = 1). Therefore, in this section, a brief review of the above issues will be given. For simplicity, the discussion will be presented separately.

2.3.1 Band gap energy bowing parameter b

As mentioned in Chapter 1, a unique characteristic of AlGaN ternary alloy is its tuneable band gap energy, namely, ranging from 3.4 to 6.2 eV. Since a precise knowledge of the dependence of the band gap on the material composition is crucial

for band gap engineering in order to realize device applications; many studies on AlGaN have been devoted to the determination of band gap energy bowing parameter b. Note that the bowing parameter b represents the deviation from a linear interpolation between the two forming binary semiconductors. Detailed description of the bowing parameter b will be given in Chapter 3.

Up to now, a number of investigations (experimental or theoretical) have been carried out to determine the values of the bowing parameter of $Al_xGa_{1-x}N$ alloy. An overview of these studies is summarized in Table 2.1. In spite of huge efforts, a consensus concerning the bowing parameter value is not yet reached owing to the results obtained by different researchers are quite diverging, as shown in Fig. 2.1. Nevertheless, the bowing parameter values reported are in the range of -0.8 to +1.56 eV, as evident from Table 2.1.

In order to explain the uncertainties of these bowing parameter values, many explanations have been proposed. It is supposed that the uncertainties are stemming from the uncertainties and peculiarities of the various techniques used to grow and to measure the band gap energy as well as to determine the alloy composition of the $Al_xGa_{1-x}N$ alloys (Ozgur et al., 2001; Ochalski et al., 1999; Teofilov et al., 2002). In other words, the derivations of b seem to be technique-dependent.

In addition, it is found that the derivations of b seem to be also growth dependent, which is a consequence of variations in growth conditions. Correlation between the measured band gaps and the methods used for epitaxial growth of the AlGaN has been investigated by Lee et al. (1999). They have found that directly nucleated or buffer growths of AlGaN initiated on sapphire at temperatures T > 800°C usually lead to stronger apparent bowing (b > 1.3 eV); while growths initiated using low-temperature buffers on sapphire, followed by high-temperature, lead to weaker bowing (b < +1.3 eV).

Table 2.1: Bowing parameter b for energy band gap E_g of $Al_xGa_{1-x}N$ thin films.

Type of study	Composition measurement	Al content, x	Thickness (μm)	Growth technique	E_g measurement	Strain state	Bowing parameter, b (eV)	Reference
Experimental	IMS, RBS and XRD	$0 \le x \le 1$	~0.15, ~0.8	MBE	LT PR	Strained	1.0	Yun et al., 2002
	XRD	$0.4 < x < 1$	0.66 – 0.82	PA-MBE	Optical trans.	Strained	0.75	Fedler et al., 2002
	XRD	$0 \le x \le 1$	0.65 – 2.0	RF-PE-MBE	LT PR and CL	NA	0.91±0.14	Teofilov et al.,2002
	EPMA and XRD	$0 \le x \le 1$	0.2 – 1.1	GS-MBE	PR	NA	1.56	Holtz et al., 2001
	XRD	$0 \le x \le 1$	0.5 – 2.0	MBE	Opt. ABS	NA	1.08	Ozgur et al., 2001
	XRD and EDS	$0 \le x \le 1$	0.25 - 5	MOCVD	UV-VIS trans.	Relaxed	1.38	Katz et al., 2001
	NA	$0 \le x \le 0.66$	0.4 – 1.5	GS-MBE	CL	NA	1.5	Nikishin et al., 2000
	RBS	$0 \le x \le 1$	0.1 – 1.0	MOCVD	Opt. ABS	NA	1.33	Shan et al., 1999
	XRD and RBS	$0 \le x \le 0.45$	~1.0	MOCVD	PL	Strained	0.69	Lee et al., 1999
						Unstrained	0.62[a]	
	NA	$0 \le x \le 0.76$	0.35-0.65	MOVPE	PL	NA	0.7	Meyer et al., 1999
	RHEED and XRD	$0 \le x \le 0.20$	NA	MOVPE	PR	NA	0	Ochalski et al., 1999

Table 2.1: (*Continued*).

Type of study	Composition measurement	Al content, x	Thickness (μm)	Growth technique	E_g measurement	Strain state	Bowing parameter, b (eV)	Reference
Experimental	XRD	$0 < x < 0.22$	0.35 – 0.65	MOVPE	PL	Strained	0.6	Steude et al., 1998
	NA	$0 \le x \le 1$	NA	ECR-MBE	SXA	NA	0	Duda et al., 1998
	XRD and ERDA	$0 \le x \le 1$	~1.0	PI-MBE	Opt. ABS	Strained	1.3	Angerer et al., 1997, Brunner et al., 1997
	XRD	$0 < x < 0.25$	0.35 – 0.65	MOVPE	ES	Strained	0.25	Takeuchi et al., 1997
	ERDA	$0 \le x \le 1$	1.0 – 1.50	MBE	UV-VIS trans.	Strained	1.3	Stutzmann et al., 1997
	XRD	$0 \le x \le 0.48$	0.02 –0.36	LP-MOCVD	UV-VIS trans. and PDS	Strained	1.48	Ambacher et al., 1997
	EDS and XRD	$0 \le x < 0.40$	0.8 – 1.8	LP-MOCVD	Opt. ABS	Relaxed	0	Wickenden et al., 1994
	EPMA and XRD	$0 \le x \le 0.40$	FM	MOVPE	Opt. ABS	NA	1.0	Koide et al., 1987
	XMA	$0 \le x \le 0.24$	FM	MOVPE	LT PL	NA	0.98	Khan et al., 1986
	EPMA	$0 \le x \le 1$	NA	MBE	Opt. Trans. and CL	NA	-0.8±0.3	Yoshida, Misawa and Gonda, 1982

Table 2.1: (*Continued*).

Type of study	Composition measurement	Al content, x	Thickness (μm)	Growth technique	E_g measurement	Strain state	Bowing parameter, b (eV)	Reference
Theoretical	Simulation (FPC)	$0 \le x \le 1$	–	–	Simulation	Relaxed	0.341# 0.351*	Liou et al., 2005
	Simulation (EPP)	$0 \le x \le 1$	–	–	Simulation	Strained	0.44	Voznyy and Deibuk, 2004
	Simulation (FP-LAPW)	$0 \le x \le 1$	–	–	Simulation	Relaxed	0.71	Dridi et al., 2003
	Simulation	$0 \le x \le 1$	–	–	Simulation	Relaxed	0.353	Kuo and Lin, 2002
	VCA	$0 \le x \le 1$	–	–	Simulation	NA	-0.08	Goano et al., 2000
	Simulation (FPLOC)	$0 \le x \le 1$	–	–	Simulation	Relaxed	0.56	Fritsch et al., 1999
	LMTO	$0 \le x \le 1$	–	–	Simulation	NA	0.34	Schilfgaarde, Sher and Chen, 1997
Theoretical and experimental	XRD and LMPP	$0 \le x \le 1$	0.5 – 2.0	PD	ABS	Strained	0.609	Deibuk, Voznvy and Sletov, 2000

Table 2.1: (*Continued*).

NA – Information not available
FM – Few microns.
FPC – First principle calculation
FP-LAPW – Full-potential linear augmented plane-wave calculations
RBS – Rutherford backscattering spectroscopy
EPP – Empirical pseudopotential
VCA – Virtual crystal approximation approach
IMS – Ion mass spectroscopy
LMPP – Local model pseudopotential
LMTO – Linear muffin-tin orbital
EDS – Energy dispersion spectroscopy
UV-VIS trans. – UV-VIS transmission
PDS – Photothermal deflection spectroscopy
Opt. trans. – Optical transmittance
LT PR. – Low temperature Photoreflectance
LT PL – Low temperature photoluminescence
PL – Photoluminescence
EPM – Electron probe microanalysis
ERDA – Elastic recoil detection analysis
XMA – X-ray micro analyses
SXA – Soft X-ray absorption
RHEED – Reflection high-energy electron diffraction
PR – Photoreflectance
CL – Cathodoluminescence
Opt. Abs – Optical absorption measurement
MBE – Molecular beam epitaxy
GS-MBE – Gas-source MBE
PI-MBE – Plasma induced MBE
PA-MBE – Plasma assisted MBE
RF-PE-MBE – Radio frequency plasma enhanced MBE
ECR-MBE – Electron cyclotron resonance assisted MBE
PD –- Pyrolytic deposition
MOCVD – Metalorganic chemical vapour deposition
LP-MOCVD – Low pressure metalorganic chemical vapour deposition
MOVPE –- Metalorganic vapour phase epitaxy
#Obtained through numerical simulation for the nonlinear lattice constant
*Obtained through numerical simulation for the linear lattice constant
[a]intrinsic bowing of the unstrained AlGaN which estimated by averaging fitted bowing parameters from different measurements made on the AlGaN layers.

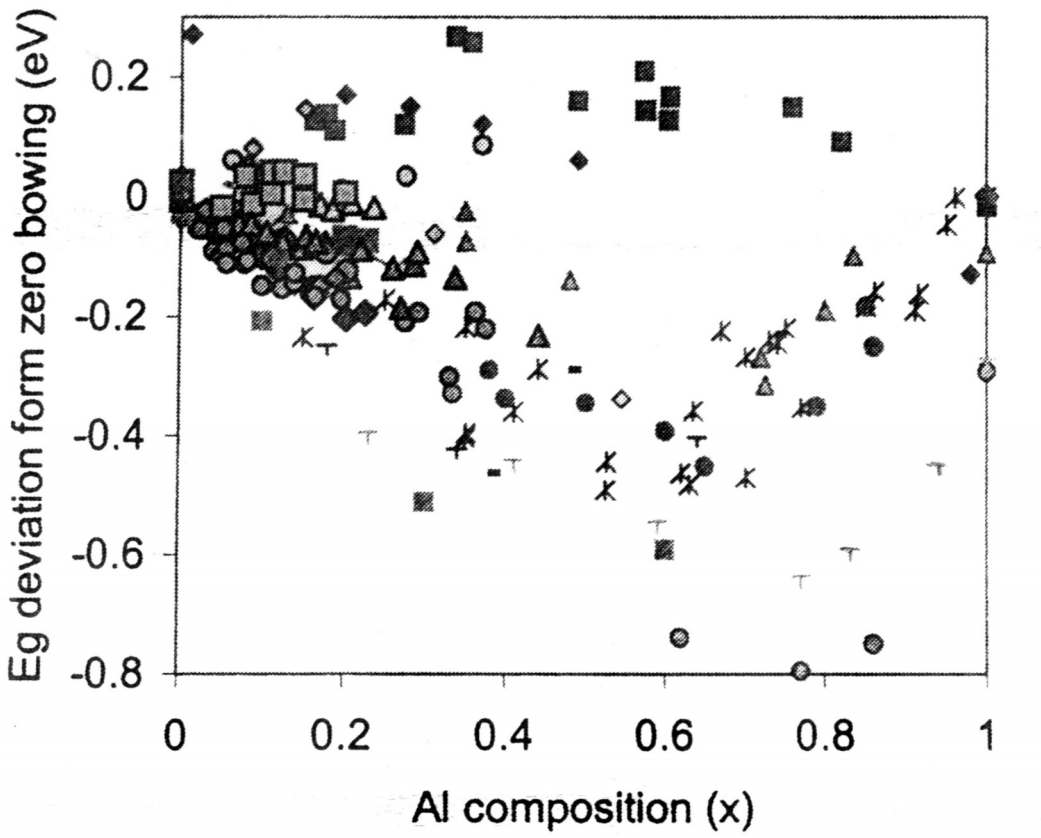

Fig. 2.1: Band gap energy of $Al_xGa_{1-x}N$ ($0 \leq x \leq 1$) versus the deviation from the zero bowing. The symbols represent the experimental data (band gap energies) from published works. (Adapted from Yun et al., 2002.)

Besides that the dispersion of bowing parameters reported by various researchers is mostly emanating from the quality (e.g., strain, uniformity of the alloy composition, defects, etc.) of the AlGaN samples (Shan et al., 1999; Katz et al., 2001; Yun et al., 2002). For instance, Vurgaftman, Meyer and Ram-Mohan (2001) have presented a brief review on the variation of band gap energy bowing parameter for AlGaN thin films due to the strain.

Other factors that cause the uncertainties in the determination of the b value are the range of alloy compositions explored being narrow (x < 0.5), structural effect, i.e., the composition-induced disorder in the bond lengths (Ferhat, Furthmuller and Bechstedt, 2002), compositional inhomogeneities (Steude et al., 1999), concentration

of free carriers (Brunner et al., 1997), non-uniformity in the energy band gap (Koide et al., 1987) and uncertainty for band gap energy of its constituent binary materials (Dridi, Bouhafs and Ruterana, 2003). Again, despite these factors, the essential factor that affects the accuracy of bowing parameter value is still not yet definitely concluded.

To summarize, it is difficult to determine an absolute bowing value which is growth- and technique-dependent. Nevertheless, through a systematic study and the utilization of various independent methods in the determination of the composition and the energy band gap of the alloys, more reliable bowing parameter with wide consensus can be attained.

2.3.2 Brillouin zone (BZ) optical phonon modes

There have been many experimental and theoretical studies on the BZ optical phonon modes of $Al_xGa_{1-x}N$ thin films. Basically, the behaviour and the composition dependence of the optical modes of $Al_xGa_{1-x}N$ alloy are subjects of considerable theoretical and experimental research interest because it reflects the lattice vibration properties, disorder in atomic arrangements, electronic properties, carrier concentration, strain and atomic composition as well as homogeneity of the alloy (Harima, 2002). In some cases, behaviour of the Raman line width, particular the line width of the $E_2(H)$ peak, of the $Al_xGa_{1-x}N$ is of interest because such an investigation provides insight into the alloy microstructure (Bergman et al., 1997). An overview of literature results on the BZ optical phonon modes of $Al_xGa_{1-x}N$ thin films is shown in Table 2.2.

Table 2.2: Optical phonon modes (in unit of cm^{-1}) for wurtzite $Al_xGa_{1-x}N$ thin films.

Method	Growth technique	Substrate (BL)	Thickness (μm)	Composition range	Phonon mode	Behaviour	Interpolation/Remark	Reference
Raman (RT and 100 K)	MBE	Sapphire (GaN)	0.5 ($0 < x < 0.5$)	$0 \le x \le 1$	$A_1(LO)$	OM	$A_1(LO) = 734 + 228x - 75x^2$ $E_1(LO) = 742 + 235x - 65x^2$ GaN-like $A_1(TO)$: $A_1(TO) = 531.8 + 62.6x + 1.9x^2$ GaN-like $E_2(L)$: $E_2(L) = 142.8 + 29x + 14.5x^2$	Davydov et al., 2002
					$E_1(LO)$	OM		
	MOCVD	Sapphire ($Al_xGa_{1-x}N$)	2.0 – 4.0	$0 < x < 0.5$	$E_2(H)$	TM		
	HVPE	Si (111) (No BL)	1.0 – 4.0	$0.5 < x < 1$	$E_1(TO)$	TM		
				$0.5 < x < 1$	$A_1(TO)$	TM		
				$0.8 < x < 1$	$E_2(L)$	TM		
Raman	PA-MBE	Sapphire (15 nm GaN)	0.66 – 0.82	$0.4 < x < 1$	$A_1(LO)$	OM	NA.	Fedler et al., 2002
					$A_1(TO)$	TM		
					$E_1(LO)$	TM		
					$E_2(H)$	TM		
Raman	AMT[a]	-	-	$0 \le x \le 1$	$A_1(LO)$	OM	$A_1(LO) = 729.1 + 349.6x - 186.9x^2$	Cao, et al., 2001
					$E_2(H)$	TM		
Raman and FTIR	GS-MBE	Si(111)	0.2 – 1.1 (40 – 60 nm AlN)	$0 \le x \le 1$	$A_1(LO)$	OM	NA.	Holtz et al., 2001
					$E_1(LO)$	OM		
					$E_2(H)$	TM		
					$A_1(TO)$	TM		
					$E_1(TO)$	TM		
Raman (RT and 100 K)	MBE	Sapphire (GaN)	0.5 ($0 < x < 0.5$)	$0 < x < 1$	$A_1(TO)$	TM	$0 \le x < 0.4$: OM $0.6 < x \le 1.0$: TM GaN-like $A_1(TO)$: $A_1(TO) = 532.5 + 58x + 55x^2$	Klochikhin et al., 2000
	MOCVD	Sapphire ($Al_xGa_{1-x}N$)	2.0 – 4.0 ($0 < x < 0.5$)					
	HVPE	Si (111) (No BL)	1.0 – 4.0 ($0.5 < x < 1$)					

Table 2.2: *(Continued)*.

Method	Growth technique	Substrate (BL)	Thickness (μm)	Composition range	Phonon mode	Behaviour	Interpolation/Remark	Reference
IRES	MOVPE	Sapphire (AlN)	0.2 – 0.8	$0 \le x \le 1$	GaN-like $E_1(TO)$	OM	NA.	Schubert et al., 1999
					AlN-like $E_1(TO)$	OM		
					$A_1(LO)$	OM		
Raman	OMVPE	Sapphire (AlN)	~2.0	$0 \le x \le 0.84$	$A_1(TO)$	OM	NA.	Demangeot et al., 1998b
					$A_1(LO)$	OM		
					$E_1(TO)$	OM		
					$E_2(H)$	OM:	Valid from $0 \le x < 0.6$	
						TM:	Valid from $0.6 < x < 1$	
FTIR	OMVPE	6H-SiC (80 nm AlN)	0.15 –0.60	$0 \le x \le 1$	$E_1(TO)$	TM	NA.	Wisniewskie et al., 1998
					$A_1(LO)$	OM		
Raman	MOCVD	Sapphire (0.5 μm GaN)	~1.5	0, 0.07, 0.15 and 1.0	$A_1(TO)$	OM	For $0 \le x \le 1$ $w(Al_xGa_{1-x}N) \approx (1+0.220x)w(GaN)$	Liu et al., 1998
					$A_1(LO)$			
					$E_1(TO)$			
					$E_1(LO)$			
					$E_2(H)$	-	Unable to detect any AlN-like $E_2(H)$ mode in the composition range of study.	
Raman (RT)	MOVPE	Sapphire (AlN)	~2.0	$0 \le x \le 0.84$	$A_1(LO)$ and $A_1(TO)$	OM (Valid for x > 0.05)	$A_1(LO) = 746 + 169.5x + 11.7x^2 - 36.6x^3$ $A_1(TO) = 540 + 19.7x + 31.7x^2 + 22.2x^3$	Demangeot et al., 1997b
					E_2	TM	NA.	

Table 2.2: *(Continued)*.

Method	Growth technique	Substrate (BL)	Thickness (μm)	Composition range	Phonon mode	Behaviour	Interpolation/Remark	Reference
Raman (300 K and 10 K)	OMCVD	6H-SiC (1000 Å AlN)	~2.0	$0 < x < 1$	$E_2(H)$	OM	$Al_xGa_{1-x}N$ of composition x = 0, 0.06, 0.12, 0.22, 0.77 and 1 are used.	Bergman et al., 1997
Raman	PE-MBE	Sapphire	~1.0	$0 \le x \le 1$	$A_1(LO)$	OM	$A_1(LO) = 736.5 + 268.3x - 125.1x^2$	Cros et al., 1997b
					$E_2(H)$	TM	NA.	
					$A_1(TO)$	-	Could not be clearly established	
Raman	PE-MBE	Sapphire	0.5 – 1.0	$0 \le x \le 1$	$A_1(LO)$	OM	NA.	Cros et al., 1997a
	MOCVD			$0 \le x \le 0.5$	$A_1(TO)$	OM		
					$E_2(H)$	TM		
Raman	MBE	Sapphire (No BL)	1.0 – 1.50	$0 \le x \le 1$	$A_1(LO)$	OM	NA.	Stutzmann et al., 1997
					$E_2(H)$	TM		
					$A_1(TO)$	OM		
Raman	MOCVD	Sapphire (AlN)	Thick bulk-like layer	$0 \le x \le 0.15$	$A_1(LO)$	OM	NA.	Behr et al., 1997
					$E_2(H)$	-	The peak become broader and no detectable frequency shift are observed.	
FTIR	MOVPE	Sapphire (35 nm AlN)	1.0 – 1.2	0, 0.08, and 0.15	$A_1(LO)$	OM	For $x \le 0.08$	Wetzel et al., 1996
Raman	MOVPE	Sapphire (50 nm AlN)	2.0 – 12.0	$0 < x < 0.15$	$A_1(TO)$	OM	NA.	Hayashi et al., 1991
					$E_1(TO)$			
					$E_2(H)$			
					$E_1(LO)$			

Table 2.2 *(Continued)*.

Method	Growth technique	Substrate (BL)	Thickness (μm)	Composition range	Phonon mode	Behaviour	Interpolation/Remark	Reference
Theoretical (MREI and RIM)	–	–	–	$0 \le x \le 1$	$E_1(LO)$ and $A_1(LO)$	OM	-	Grille, Schnittler and Bechstedt, 2000
	–	–	–		$E_1(TO)$	TM	-	
	–	–	–		E_2 and $A_1(TO)$	OM	-	
Theoretical (MREI) and experimental (Raman)				$0 \le x \le 1$	$A_1(TO)$ and $A_1(LO)$	OM		Liu, Bursill and Prawer, 2001
					$E_1(TO)$ and $E_1(LO)$	OM		
					$E_2(H)$	OM: TM:	Theoretical results. Experimental results.	

BL – Buffer layer.
RT – Room temperature
MOVPE –- Metalorganic vapour phase epitaxy
MBE – Molecular beam epitaxy
MOCVD – Metalorganic chemical vapour deposition
HVPE – Hydride vapour phase epitaxy
OMCVD – Organometallic chemical vapour deposition
PE-MBE – Plasma-enhanced MBE
FTIR – Fourier transform infrared spectroscopy
GS-MBE – Gas-source MBE
PA-MBE – Plasma-assisted MBE
IRES – Infrared ellipsometry spectroscopy
MREI – Modified random-element isodisplacement
RIM – Rigid-iron model
OM – One mode behaviour
TM – Two modes behaviour
NA – Not available.

[a]Nanocrystalline solids with an average size of 40 nm are formed

In general, most of the studies are performed by using Raman methods. This is because Raman spectroscopy is a direct technique for the observation of optical phonons as compared to the IR and IRE spectroscopy. Unlike the Raman approaches, a fitting procedure is normally needed to extract the phonon frequencies from the IR and IRE spectra. The work of extraction may become complicated if the reststrahlen band (IR absorption band) of the concerning layer is superimposed with that from the underlying layer. Nevertheless, in some aspect, the IR or IRE spectroscopy is preferred than the Raman scattering. For instance, they are sensitive to the IR-active lattice vibration modes as compared to Raman scattering measurement.

There have been several reports/reviews on the behaviour and the composition dependence as well as the line width of the optical modes of $Al_xGa_{1-x}N$ alloy (Harima, 2002; Haboeck et al., 2003; Kuball, 2001; Wetzel and Akasaki, 1999). However, only a brief description is given because most of the attention is paid to its constituent materials, namely, the GaN and AlN. A comprehensive Raman scattering and theoretical study has been reported by Davydov et al. (2002) and Grille, Schnittler and Bechstedt (2000), respectively. Therefore, the following discussion mainly refers to the results given in the cited literature.

For wurtzite structures of GaN and AlN, there are six BZ centre optical phonon modes which are IR or Raman active, or active under both investigations, namely, $A_1(TO)$, $A_1(LO)$, $E_1(TO)$, $E_1(LO)$, $E_2(L)$ and $E_2(H)$. Like its parent, wurtzite structure AlGaN also consists of these sets of BZ centre optical phonon modes, however, the situation is more complicated. In some aspect (depends on the alloy composition), these optical phonons may exhibit either a “one-mode” (OM), a “two-mode” (TM) or a “mixed-mode” (MM) behaviour. Note that detail descriptions of the behaviour of these modes will be given in Chapter 3.

A general picture of the behaviour of some BZ centre optical phonon modes as a function of alloy composition has been obtained through the theoretical study by Grille, Schnittler and Bechstedt (2000), as shown in Fig. 2.2. The composition

dependence of the phonon frequencies of all the six BZ centre optical phonon modes of wurtzite $Al_xGa_{1-x}N$ obtained through the Raman scattering study by Davydov et al. (2002) is shown in Fig. 2.3. It important to note here that Fig. 2.2 and Fig. 2.3 given here are used for reference purposes only, because there may be some discrepancies between these results.

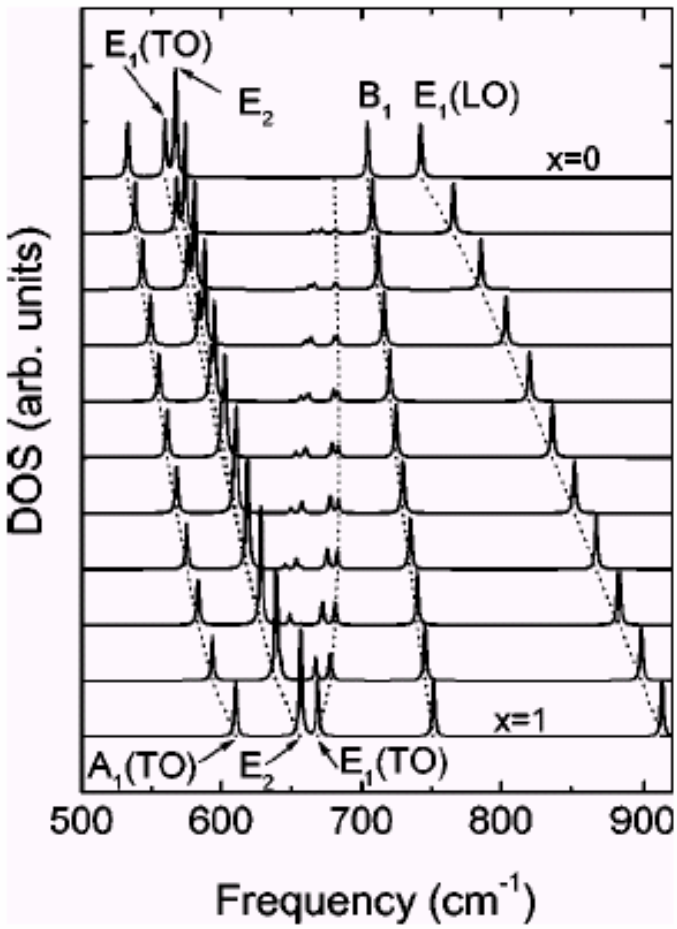

Fig. 2.2: Behaviour of the BZ centre phonons in wurtzite $Al_xGa_{1-x}N$ as a function of alloy composition with the phonon propagation direction perpendicular to the C-axis. The vertical axis represents the density of states (DOS) for the BZ centre phonons. (Adapted from Grille, Schnittler and Bechstedt, 2000.)

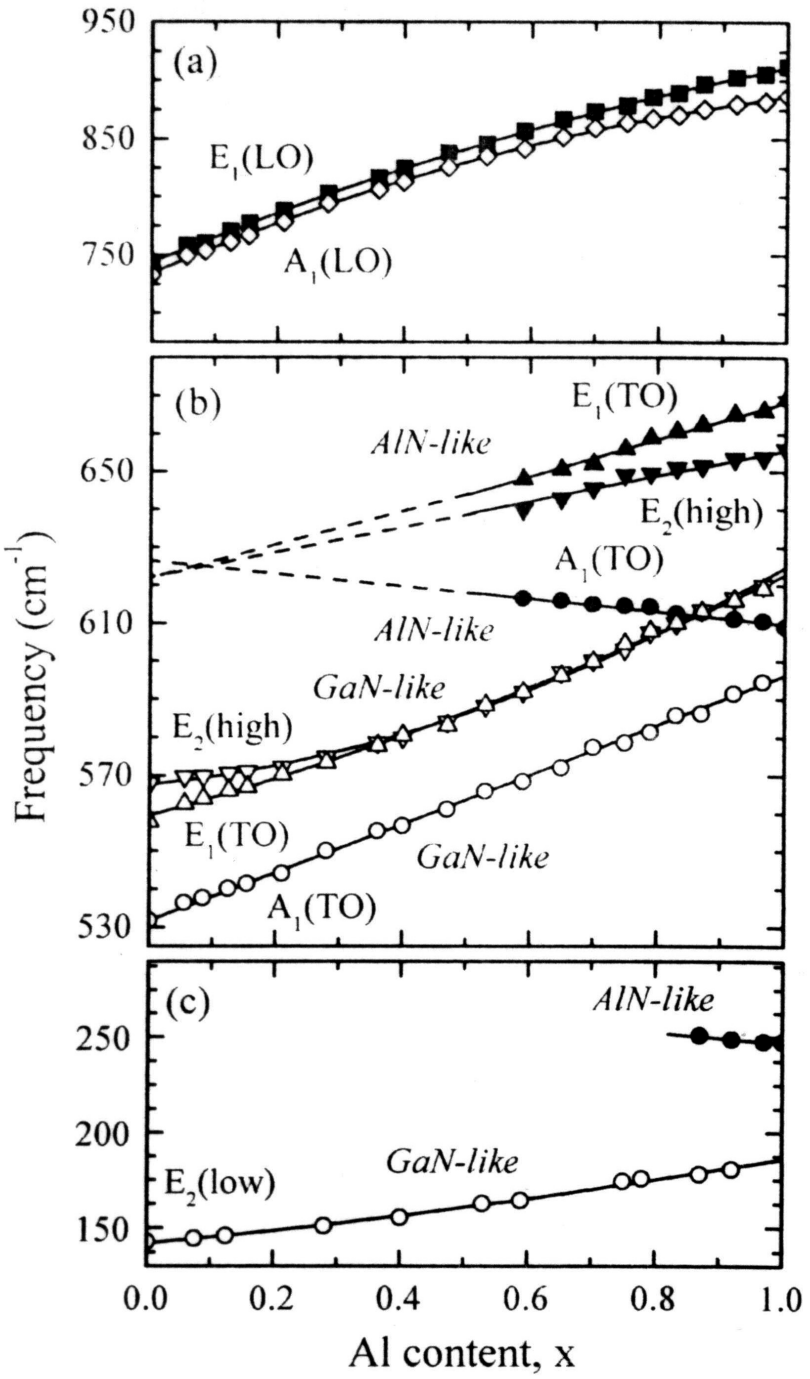

Fig. 2.3: Composition dependence of the BZ centre optical phonons in wurtzite $Al_xGa_{1-x}N$. (Adapted from Davydov et al., 2002.)

Based on the literature results in Table 2.2 the behaviour of the BZ centre optical phonon modes of the $Al_xGa_{1-x}N$ alloys is evaluated and summarized in Table 2.3.

Table 2.3: An evaluation (based on the literature results) of the behaviour of the BZ centre optical phonon modes of the $Al_xGa_{1-x}N$ alloy over the entire composition range ($0 \leq x \leq 1$).

Phonon mode	Behaviour	Remark
$A_1(TO)$	OM	➢ No consensus is reached concerning the behaviour of this mode. ➢ This conclusion is made after considering the theoretical results.
$A_1(LO)$	OM	➢ A consensus is reached in all the reported results.
$E_1(TO)$	TM	➢ A broad consensus is reached.
$E_1(LO)$	OM	➢ A broad consensus is reached.
$E_2(L)$	TM	➢ There is only one reported result on this mode.
$E_2(H)$	TM	➢ A broad consensus is reached.

OM – One-mode behaviour.
TM – Two-mode behaviour.

For $A_1(LO)$ mode, all the reported results reveal a OM behaviour. In contrast, the behaviour of the $A_1(TO)$ mode still remains a controversial issue and is a subject of ongoing debate in the literature. This is because both OM and TM have been observed and no consensus is attained among the reported results. An explanation of this issue has not yet been reported. Note that the conclusion, of OM behaviour, is made after taking into account the theoretical results.

A broad consensus is reached between the literature results on the behaviour of the $E_1(LO)$ and $E_1(TO)$ modes, where OM and TM behaviour are, respectively, concluded. Last but not least, a TM behaviour for both $E_2(L)$ and $E_2(H)$ modes is deduced. It is interesting to point-out here that there is only one paper that reported the behaviour of the $E_2(L)$ mode.

On the subject of the composition dependence equation of the optical phonon modes, it can be concluded from Table 2.2 that less attention is paid on this subject. Moreover, it is found that there are no consensuses between the reported results on the derived composition dependence equations.

Another subject of interest on the Raman scattering results of AlGaN alloy is the behaviour of the Raman peak line width. An earlier Raman analysis on the $E_2(H)$ mode

of $Al_xGa_{1-x}N$ by Bergman et al. (1997) revealed that the Raman line shape exhibit a significant asymmetric broadening for x > 0.6. This Raman line broadening is then attributed to the activation of phonons wave vector $\boldsymbol{q} \geq 0$ arising from the disordered state of the alloys. In addition, they found that the maximum line broadening of the $E_2(H)$ mode at composition $x \approx 0.5$ is an indicator for the disorder state. Cros et al. (1997b), however, observed a maximum line broadening at $x \approx 0.8$. This discrepancy arises most probably due to the difference in the samples quality.

Recently, the composition dependence of the Raman lines [$A_1(TO)$, $A_1(LO)$, $E_1(TO)$, $E_1(LO)$ and $E_2(H)$] broadening has been investigated theoretically and experimentally by Davydov et al. (2002) and the results are shown in Fig. 2.4. They found that all the lines exhibit an asymmetry broadening with respect to the point x = 0.5, however, the asymmetric broadening pattern for the $A_1(LO)$ and $E_1(LO)$ modes is skewed to the left, while that for the $A_1(TO)$ and $E_1(TO)$ modes is skewed to the right. The line width of the $E_2(H)$ mode has a less asymmetrical composition dependence. The alloy composition at which these lines exhibit a maximum line width are different, namely, at $x \approx 0.65$ to 0.7 for $A_1(TO)$ and $E_1(TO)$, $x \approx 0.35$ for $A_1(LO)$ and $E_1(LO)$, and $x \approx 0.75$ for $E_2(H)$. However, no explanation is given on these phenomena. Hence, there is a need for more research on these phenomena.

From the brief review above, one can conclude that the behaviour and composition dependence as well as the line width of the BZ optical phonon modes (except the $A_1(LO)$ mode) of the $Al_xGa_{1-x}N$ is still unclear. More work is needed to address these issues.